JOURNAL OF MATERIALS SCIENCE **34** (1999) 1667–1680

Effect of interface chemistry on the mechanical properties of Si_3N_4-matrix composites

G. PEZZOTTI, T. NISHIDA
Department of Materials, Kyoto Institute of Technology, Matsugasaki, 606-8585 Kyoto, Japan
E-mail: pezzotti@chem.kit.ac.jp

H.-J. KLEEBE
Institut fur Materialforschung, Universitat Bayreuth, Ludwig-Thoma Strasse 36B, D-95440 Bayreuth, Germany

K. OTA
The Institute of Scientific and Industrial Research, Osaka University, Mihogaoka 8-1, Ibaraki-shi, Osaka 567, Japan

N. MURAKI
Toray Research Center, Inc., Sonoyama 3-3-7, Otsu-shi, Shiga 520, Japan

V. SERGO
Materials Engineering and Applied Chemistry Department, University of Trieste, Via Valerio 2, 34127 Trieste, Italy

The effect of systematic modifications in the chemistry of the phase-boundary film on the macroscopic mechanical properties of Si_3N_4-matrix composites was investigated. Model composite materials, containing SiC or WC platelets, were prepared and only the bulk anion composition of the glassy-SiO_2 intergranular phase was varied by adding increasing amounts of fluorine to the material. Detailed material characterizations by high-resolution electron microscopy (HREM) and Raman spectroscopy on both undoped and F-doped composites allowed to derive a structural model of the phase-boundary film as well as to evaluate the average microscopic stresses acting on it. In addition, high-temperature internal friction measurements provided an estimate of the grain-boundary relaxation temperature as a function of the F content. Noticeable variations of both elastic modulus and fracture energy of the composite were detected upon F addition, which were related to a spontaneous process of phase-boundary microcracking upon cooling. A threshold of the F-content was found for microcrack formation and its existence is theoretically explained according to a percolation process of non-bridged SiO_4-tetrahedra, which arises from the incorporation of F into the intergranular film network.

1. Introduction

Only few systematic studies were yet reported in literature, which relate the intrinsic fracture energy of grain- and phase-boundaries to the macroscopic mechanical properties of ceramic composites. One main reason for the lack of such basic data undoubtedly resides in the scarce availability of simple (i.e., model) composite systems. As a matter of fact, the majority of fracture mechanics studies on toughened ceramics were performed on materials of rather complex composition, designed for other purposes or very specific applications. A typical example may be that of Si_3N_4 ceramics and related composites. Because of its inherently slow diffusion rate and liability to decomposition at high temperatures, the Si_3N_4 is commonly (and often empirically) added with several metal oxide phases to achieve full densification. Hence, the complexity of the system is increased since a variety of chemical and physico/chemical parameters become additionally involved in the micromechanical behavior of the material which make difficult the prediction of any toughening effect. Early phenomenological studies on the topic [1, 2] suggested that geometrical parameters, such as grain diameter and aspect ratio, can mainly be responsible for toughening effect. However, it was successively noticed that Si_3N_4-based materials, with the same geometrical characteristics, may show noticeably different values of fracture toughness [3]. This means that the effect of grain size and morphology is necessarily vinculated by, at least, one further important parameter: the grain-boundary bond strength. Although the effect of the inter-granular phase on the fracture toughness of Si_3N_4 ceramics is yet to be fully understood, it is worth citing a recent systematic study by Peterson and Tien [4], in which emphasis was placed on the dependence of toughness on residual microstresses arising from the

thermal expansion mismatch between Si_3N_4 grains and different grain-boundary phases. The overall fracture resistance of the Si_3N_4 material increased as the inherent thermal expansion coefficient of the grain-boundary phase increased. In other words, the presence of a tensile residual stress of increasing magnitude at the grain boundary (e.g., caused by a higher thermal expansion coefficient of the grain-boundary phase as compared to the matrix grains) enhances the crack debonding process and allows toughening mechanisms to become operative.

In addition to the study reported by Peterson and Tien [4], we investigate here the effect of grain-boundary structure, which is strongly affected by its local chemistry, on the fracture behavior of two Si_3N_4-matrix SiC- and WC-platelet-reinforced composites. In the present model materials, with fixed morphological parameters, the bond strength of the glassy phase, present at grain and phase-boundaries, was systematically varied by doping with increasing amounts of fluorine impurity.

One basic observation behind the present investigation was that it is not easy to explain whether microscopic interface debonding occurs or not by simply invoking a change in the *inherent* fracture energy of the grain-boundary phase. This is because the intrinsic fracture energy of glassy materials hardly varies drastically according to small chemical changes.* Hence, there should be some basic effect of micromechanical nature which "amplifies" the influence of grain boundary chemistry and, by affecting the microfracture behavior of the composite, dominates the overall material toughness. Certainly, one kind of such an "amplification" factor can be the mismatch in thermal expansion between the Si_3N_4 matrix grains and the glassy film, as indicated by Peterson and Tien [4]. However, the present results on model materials provide evidence that other grain-boundary chemistry-related parameters, such as grain-boundary relaxation temperature and modified network geometry of the glass structure, also play an important role on the macroscopic fracture behavior of the material.

2. Basic experimental approach and tools

It is known that SiO_2, as an impurity, is generally present in Si_3N_4 ceramics due to surface oxidation during exposure to atmosphere. Pure SiO_2 in the glassy status exists at grain and phase-boundaries of Si_3N_4-based materials, when they are densified without external addition of sintering aids [5, 6]. This is also the case of the Si_3N_4-matrix composites investigated in this study. The SiO_2-glass phase is found to typically circumvent the grains as a continuous film with a thickness of 1.0 nm [7]. A mole fraction of nitrogen (typically $\approx$6 at %) may also be found in the SiO_2 glass [7, 8], as a consequence of the solution-precipitation process which occurs during liquid-phase sintering of Si_3N_4. However, it has previously been shown [8] that such a small amount of nitrogen, which may also represent the solubility limit of N in pure SiO_2 [9], involves only limited modifications of both the SiO_2-network structure and the bulk properties of the present materials. Hence, the influence of N atoms in the glassy-SiO_2 film will not be considered in the present study. Additions of F-dopant remain entirely segregated at the grain-boundary, as recently shown by the authors [10–12], since F atoms have no appreciable solubility in the β-Si_3N_4 lattice. In this study, some evidence of F segregation at the phase-boundaries of Si_3N_4-matrix composites will be provided and its amount estimated by spectroscopy microanalysis.

The addition of F to the composite generally involves only a small increase in grain-boundary film thickness (i.e., $\Delta h \approx 0.1$ nm), as compared to the pure material, while modifications of both grain size and morphology cannot generally be detected [10–12]. Image analysis data, collected on large sectional areas [13] of the present composites, have shown that, owing to the isostatic processing procedure adopted in this study (i.e., cold isostatic pressing (CIP) followed by HIPing), the platelet dispersoids remain randomly distributed within the sintered body. Furthermore, the average platelet dimensions were found to be not significantly altered by the HIP process, as compared to the starting powders.

Since the undoped samples showed a rather strong interface bond strength [14, 15], a negligible effect of thermal expansion mismatch between the SiO_2 and Si_3N_4 phases is assumed in the present composites. In addition, marked variations in both thermal expansion and *inherent* fracture energy of the SiO_2 glass upon F addition can be reasonably excluded. Hence, basically, in our experimental approach, only the structure and local chemistry of the glassy-SiO_2 phase was varied.

Microscopic and mechanical analyses are described to adequately characterize the microstructure and to relate it to the fracture behavior of the present composites. In addition, further insight in the fracture behavior of the composites is provided by both Raman spectroscopy and internal friction analyses. The possibility to directly determine residual microstresses in Si_3N_4-based materials by Raman spectroscopy has recently been demonstrated by the present authors [16, 17]. Here, we apply the Raman technique in order to estimate the phase-boundary bond strength. Furthermore, one important parameter needed for the theoretical assessment of residual microstresses is the grain-boundary relaxation temperature, ΔT. This parameter was also directly measured by monitoring the shift of the grain-boundary relaxation peak of internal friction as a function of the F content in the present composites. These experiments were performed with a newly developed torsional pendulum apparatus which allows both internal friction and elastic modulus measurements up to very high temperature [18–20].

3. Experimental procedures

3.1. Model materials

The starting Si_3N_4 powder used for preparing the present model materials was a high-purity, commercially

* The basic assumption that the inherent fracture energy of the SiO_2 boundary is not markedly changed by fluorine addition has originally been suggested by Dr. S. Wiederhorn who we gratefully acknowledge.

available powder (E-10, Ube Ind. Ltd., Ube, Japan), whose total amounts of cation impurities and oxygen were <0.01 wt % and 1.3 wt %, respectively. Two kinds of platelet-shaped ceramic reinforcements, with the same average size of 25 μm, were added to the Si_3N_4 matrix with a constant volume fraction of 25%: (I) α-SiC (C-Axis, Jonquiere, Canada), and (II) WC (Nihon Shin Kinzoku, Osaka, Japan). The aspect ratios ranged between 5 and 8 for both the platelet phases. In comparison with these undoped materials, three specimens (per each composite system) with identical phase assemblage but doped with different amounts of F were also prepared. The F-dopant was introduced into the composites by adding an increasing amount of pulverized polytetrafluoroethylene (Teflon, E.I. du Pont de Nemours, Wilmington, DE) during the mixing procedure of the powders. Powder blends were then pre-fired in high vacuum at 1200 °C, in order to depolimerize Teflon to tetrafluoroethylene C_2F_4 and, successively, to eliminate the forming CO gas. Teflon was chosen as the starting compound to introduce F into the material since it does not involve the contemporary incorporation of H into the specimen and, hence, allows an easier modelling of the grain-boundary SiO_2 structure at which only F remains segregated. It should be noted that it was difficult to introduce F-amounts larger than about 0.2 wt % by the present procedure.

Mixing of the raw powders was performed in ethanol with a rotary evaporator immersed in an ultrasonic bath to promote an intimate dispersion of the constituent phases. Powder compacts were prepared by cold-isostatic-pressing (CIP) at 200 MPa, coated by BN powder, subsequently prefired *in vacuo* (10^{-5} Pa) at 1200 °C, and finally encapsulated into an evacuated tube of borosilicate glass. The HIP cycles were carried out for 1 hour at 2050 °C. An isostatic pressure of 180 MPa was externally applied via Ar gas. The above conditions for HIP sintering allowed to obtain fully dense samples (density > 99.5%). The F content in the sintered body was measured by ion-selective electrode (ISE) method after dissolving the specimens in NaOH.

For assessing the inherent fracture properties of the intergranular glass upon F addition, undoped and F-doped bulk glass specimens were also prepared. High-purity SiO_2 powder (Hokko Chemical Co., Ltd., Osaka, Japan) was first mixed with appropriate amounts of Teflon (leading to the same nominal glass composition of the intergranular phase of the composites) and then HIPed at 1800 °C, under 130 MPa, in Ar atmosphere, in order to obtain dense bodies.

3.2. Fracture mechanics and internal friction measurements

Fracture mechanics characterization of the composites was performed on chevron-notched specimens loaded in three-point bending geometry with a cross-head speed of 0.01 mm/min. The span width was 45 mm. The parameter selected for representing composite toughness was the work of fracture (WOF). It was determined from the area subtended by the stable load-displacement curve after dividing by twice the ligament fractured area. This latter area was measured by *post mortem* fractography. Further details on the fracture mechanics characterization have been reported elsewhere [21]. The fracture toughness (K_{Ic}) of the bulk SiO_2 glass, as a function of the F-content, was measured by the single-edge pre-cracked beam method in bending geometry [22].

The grain-boundary relaxation temperature, ΔT, as a function of the amount of F in the glassy-SiO_2 grain-boundary phase, was determined from the anelastic grain-boundary peak of internal friction of the Si_3N_4/SiC composites. The apparatus used for measuring simultaneously the internal friction, Q^{-1}, and the shear modulus, G, was of the torsion pendulum type, similar to that used by Kê [23]. The specimen dimensions were $2 \times 3 \times 50$ mm. The apparatus was enclosed in a vacuum-tight system where a controlled argon atmosphere could be mantained throughout the experiments. A carbon heater, surrounding the specimen, was employed to raise the testing temperature. The absolute strain amplitude was calibrated prior to testing by a strain gauge attached to the sample surface. It corresponded to an outer-fiber maximum stress of 10 MPa. Measurements were performed at the frequency of 10 Hz according to the free decay method [24]. Calibration by the strain-gauge method at room-temperature revealed a confidence of ± 1 GPa in the measurement of G values.

3.3. Microscopy and spectroscopy experiments

The grain- and phase-boundaries of the composites were characterized by HREM experiments using a 400-kV transmission electron microscope (Model 4000EX, JEOL, Tokyo, Japan) with a point resolution of 0.18 nm when operated at 400 kV. TEM foils were prepared by the successive procedures of grinding, dimpling, and argon-ion-beam thinning of the sintered bodies, followed by light carbon coating to avoid charging during HREM observations. The technique adopted to quantitatively measure the grain boundary thickness has been previously described [25].

The actual presence of F in the glassy-SiO_2 intergranular phase was determined by electron energy-loss spectroscopy (EELS) with the spectrometer (Gatan, Model 666, Warrendale, PA) attached to a Philips CM20FEG scanning/transmission electron microscope, operating at 200 kV using a probe size of about 1–2 nm.

In this study, Raman spectroscopy was adopted for measuring internal residual microstresses in the densified specimens. Frequency shifts of Raman bands were monitored and analyzed to determine the average hydrostatic stress in both the SiC-platelet and Si_3N_4-matrix phases. An argon ion laser operating at a wavelength of 488 nm with a power of 300 mW was used as the excitation source; an optical microscope was employed to focus the laser on the sample and to collect

the scattered frequencies, which were then analyzed using an attached spectrometer (T 64000 Jovin-Yvon, ISA). The scattered light was analyzed with a triple monochromator equipped with a charge-coupled device (CCD) camera. The dimension of the laser spot on the samples was 100 μm. A neon discharge lamp was used for an external frequency calibration. A standard temperature calibration procedure was also followed in order to correct the error which may arise from slight variations of the room-temperature. Further details about the Raman spectroscopy measurements are given elsewhere [16]. The collected data were analyzed with curve-fitting algorithms included in the SpectraCalc software package (Galactic Industries Corp.). The piezo-spectroscopic coefficients relating the shift of the Raman bands (794.1 and 970.8 cm^{-1}) to the uniaxial stress field in α-SiC were found in the literature [26–28]. The piezo-spectroscopic coefficients of the high-frequency shift bands of β-Si_3N_4 (namely the 862, 925 and 936 cm^{-1} Raman bands) were recently determined by the present authors [16]. Data on the shift of the 862 cm^{-1} Raman band, which is also the Raman band with the highest piezo-spectroscopic coefficient for β-Si_3N_4 crystals [16], were mainly employed for calculating the residual stress in the matrix material.

4. Results

Electron microscopy inspections on the sintered bodies showed that the F addition did not alter significantly the microstructure of the matrix materials, the morphology of the matrix grains being typically equiaxed and the average grain-size approximatively 1 μm. A characteristic low-magnification TEM micrograph and a HREM image of the Si_3N_4/SiC phase-boundary in the composite doped with $\approx$0.1 wt % F are shown in Fig. 1A and B, respectively. HREM images of the Si_3N_4/Si_3N_4 grain-boundary structure have previously been shown [10–12]. Typical features of the composite microstructure are envisaged in micron-sized Si_3N_4 grains surrounding large SiC platelets. High-magnification inspection of phase boundaries reveals an amorphous interphase with a thickness of about 4–5 nm. The inset of Fig. 1B shows the result of EELS analysis which confirms the actual presence of F at this phase-boundary. F is a known modifier of the SiO_2-glass network, forming non-bridging Si-F bonds in the glass structure. According to the measured thickness of the phase boundary depicted in Fig. 1B, the SiO_2 structure should basically be constituted of few tens SiO_4 tetrahedra. F and O atoms, the latter being replaced by the former in the present experiments, have almost identical ionic radii (0.140 nm against 0.133 nm) but different ionic valency. To gain charge neutrality, one O^{2-} ion must be replaced by two F^- ions, which leads to a small widening of the interlayer [10–12]. It is important for the purpose of this paper to notice that the presence of F-ions in the SiO_2 network will necessarily lead to non-bonded SiO_4 tetrahedra (cf. inset in Fig. 1B), which are thought to play a fundamental role in the microfracture process of these composites. This point will be discussed in a following section. Similar EELS spectra were recorded from grain boundaries, phase boundaries as well as triple-grain junctions. Hence, it was assumed that, at first approximation, a homogeneous SiO_2-glass composition is present within these F-doped composites. The proposed structure of the glassy phase for which, apart from the thickness of the intergranular film, almost no informations were available from the HREM images, is given in the inset of Fig. 1B.

One main consequence of the incorporation of F atoms in the grain and phase boundaries of the materials is the lowered viscosity of the SiO_2 glass. This point has been discussed previously [10]. In this paper, we will deal with the influence that such a lowered viscosity may have on the residual microstresses stored in the composites upon cooling down from the HIPing temperature. Fig. 2A shows the grain-boundary relaxation peaks, as found in the present Si_3N_4/SiC materials, as a function of the F content. The F addition is found to lower the peak-top temperature (Fig. 2B) and, concurrently, to broaden the peak shape. Since the peaks were detected with testing the internal friction of the composites at a constant frequency of $\approx$10 Hz, the viscosity of the grain and phase-boundary SiO_2 glass experiences value of $\approx 10^7$–10^8 Pa $\cdot$ s [10], at the peak-top temperature shown in Fig. 2B. In this study, we have assumed such a viscosity value as the lowest limit for which considerable sliding is allowed and the stresses at the interfaces can be relaxed. Hence, the elastic stress-free temperature (on cooling), ΔT, was taken to be approximately the same as the peak-top temperature, T_R. This practice clearly represents an approximation since the external application of local stresses on the grain boundaries during the internal friction measurements occurs at a finite strain rate (depending upon the measurement frequency), while the external stress applied during cooling down from HIPing temperature is constant. From this point of view, the elastic stress-free temperatures, ΔT, as determined in this study, may only represent the upper limits of their actual values. However, the present approach for selecting the ΔT values provides a rationale for taking the dependence of ΔT on the F content into account. Furthermore, as we shall show afterwards, such an approximation leads to physically reasonable results with respect to the present composites. This may also be due to the low frequency (i.e., low strain rate) at which the internal friction was measured.

The dependence of toughness, WOF, and shear modulus, G, of the composites on the amount of F dopant, x_F, is shown in Figs 3 and 4, respectively. The toughness trends (Fig. 3), similar for both SiC- and WC-reinforced composites, can be fitted by a single curve, which shows a pronounced maximum at around 0.1 wt % F content. In other words, it is found that a large addition of F leads to a pronounced decrease in WOF. The shape of the toughness curve is very similar to those reported by Fu and Evans [29] for several polycrystalline ceramics, which undergo extensive grain-boundary microcracking processes. It is conceivable to suspect that microcrack formation occurs also in the present composites since the thermal expansion

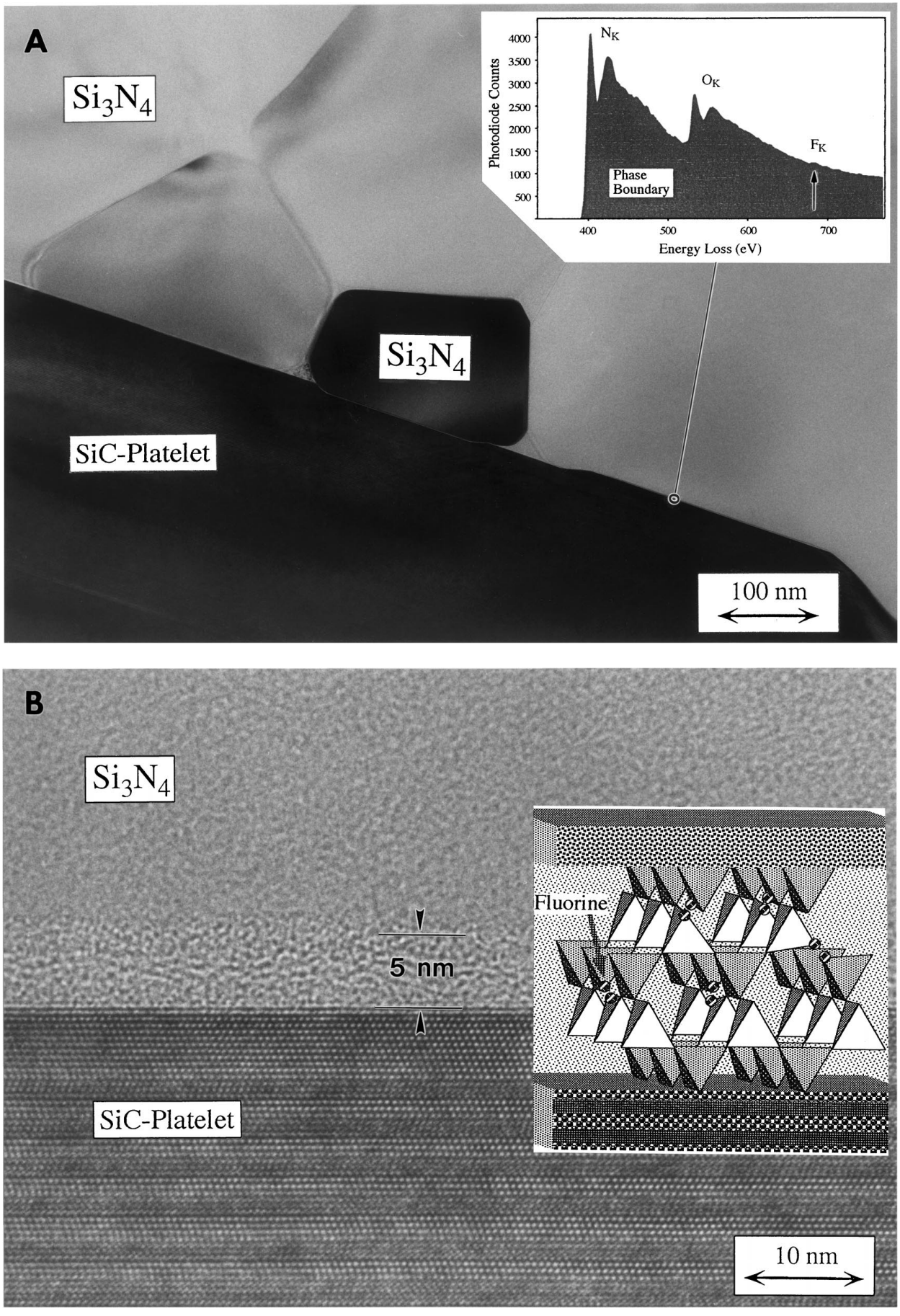

Figure 1 (A) Characteristic low-magnification TEM image of the Si_3N_4/SiC-platelet composite containing 0.104 wt % F. A nearly flat edge of a large SiC platelet is surrounded by the fine grained Si_3N_4 matrix. Note that the microstructure of the F-doped samples was undistinguishable from that of the undoped sample on the scale of this micrograph. EELS analysis, shown in the inset, reveals the presence of a minor fraction of F, together to N and O, at the phase boundary (carbon, with an energy-loss of 284 eV is not shown). (B) HREM micrograph of a Si_3N_4/SiC-platelet phase boundary. A continuous amorphous SiO_2-film is present along the interface, with a thickness of ≈4–5 nm. Note that the phase boundaries are typically wider compared with the Si_3N_4/Si_3N_4 grain boundaries [10-12]. The inset shows a guessed model of the phase-boundary structure in presence of F-dopant.

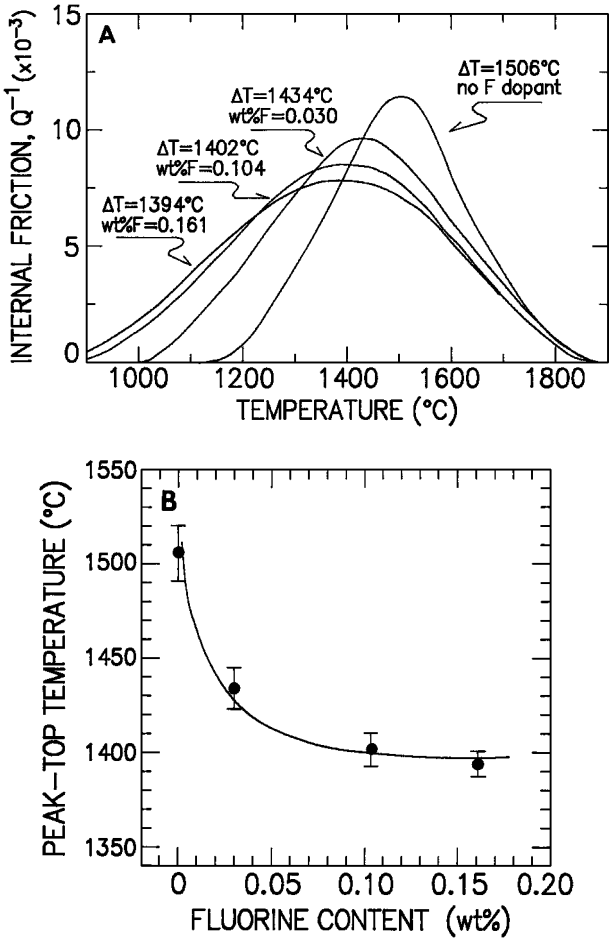

Figure 2 (A) Temperature shift of the internal friction peak for the Si_3N_4/SiC-platelet composite [10], as a function of the F content. For clarity, the respective peak-top (relaxation) temperatures are replotted in (B), as a function of the F content.

coefficient of the SiC- and WC-platelet dispersoids is larger than that of the matrix grains. This point will be clarified by TEM and Raman spectroscopy data, as shown afterwards. The dependence of shear modulus on F content (Fig. 4) may also confirm the microcracking hypothesis, since a marked drop-down in the material stiffness is noticed for large additions of F dopant.

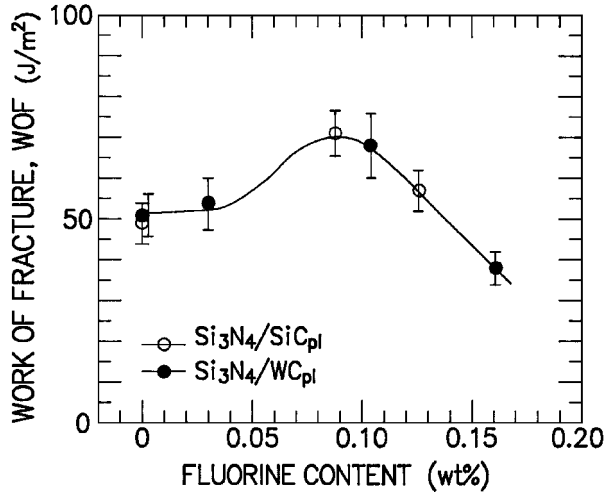

Figure 3 Dependence of the macroscopic work of fracture, WOF, of the Si_3N_4/SiC and Si_3N_4/WC composites on the F content.

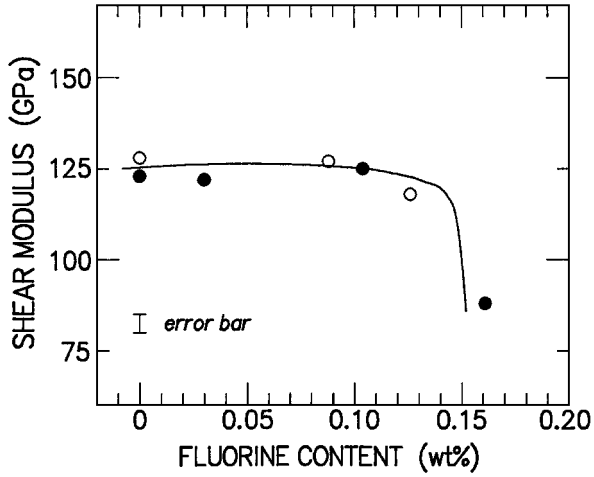

Figure 4 Dependence of the shear modulus, G, of the Si_3N_4/SiC and Si_3N_4/WC composites as a function of the F content.

In order to verify the actual formation of microcracks upon F addition, the Si_3N_4/SiC composite specimens containing 0.03 and 0.16 wt % F were observed by TEM. In the latter specimen, extensive presence of microcracks was detected at the Si_3N_4/SiC phase-boundaries (Fig. 5), while the matrix grain-boundaries were hardly found to be fractured. Microcracks were not detected in the low-doped composite.

The (average) residual microstresses acting on the platelet dispersoids and the phase boundaries were measured by Raman spectroscopy. Fig. 6 shows the dependence of such stresses on the F content. In the Si_3N_4/SiC materials, the Raman technique allowed to directly determine the stresses in both constituent phases of the composites. Hence, the error involved with the residual stress determination could be verified by applying the equation of internal equilibrium to the composite microstructure (i.e., Equation 3 to be shown in the following section). Error bars are thus plotted for this material in Fig. 6. The stress in the WC phase could not be directly determined since the stress dependence of the Raman spectrum of this ceramic phase is presently unknown. Hence, the data plotted in Fig. 6 for the Si_3N_4/WC materials were indirectly calculated from stress data measured in the Si_3N_4 matrix through equilibrium equations, and the error involved with these values could not be evaluated as done for the Si_3N_4/SiC composite. As seen, significant tensile microstresses are found to be stored in the platelets which, acting on the phase boundary, can promote opening of microcracks. The residual stress values in both composites appear to experience a non-linear decrease up to ≈15% of F content. Again, a marked drop-down is noticed for large F-addition. This drop-down clearly reflects, as confirmed by TEM observation, the presence of a conspicuous microcracking process in these materials. The microcracks, present only at the phase boundaries can locally release the stored tensile microstresses and thus lower markedly the measured (average) residual stress value as compared to composites containing lower amounts of F.

The above set of microscopy, spectroscopy, and mechanical data seems to suggest that there is a critical

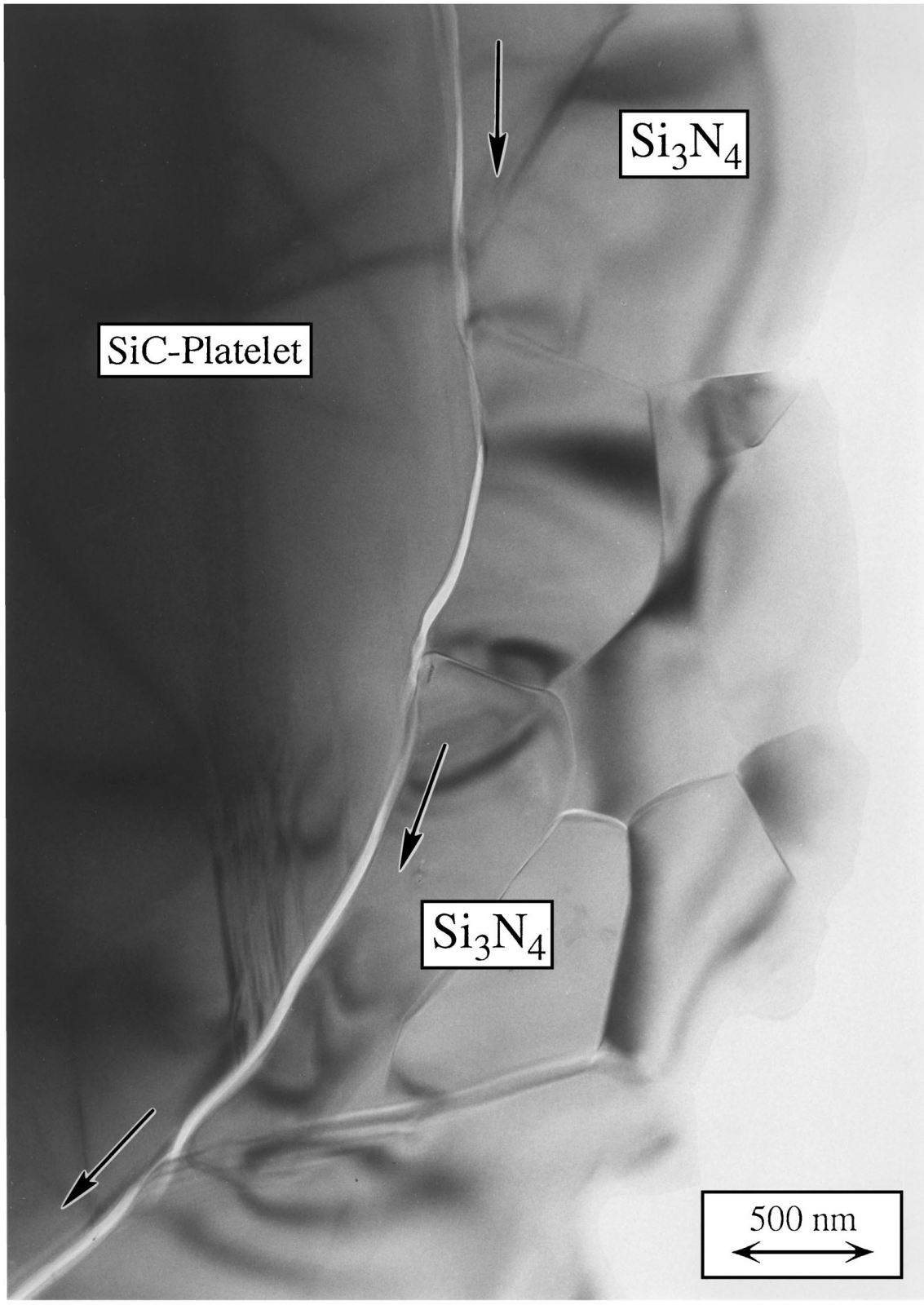

Figure 5 Low-magnification TEM micrograph of a phase-boundary spontaneously cracked after cooling, as observed in the Si_3N_4/SiC composite doped with 0.104 wt % F. Some of the SiC platelets were found to be nearly completely circumvented by cracked boundaries. Such a microcracking process could be envisaged only in the samples doped with larger amounts of F.

amount of F, x_F^*, in the SiO_2 phase (i.e., in the range 0.1–0.2 wt %), over which an extensive process of spontaneous (i.e., upon cooling from sintering temperature) microcracking takes place within the polycrystal. This hypothesis will be theoretically explored in the following sections and the actual role of the boundary-phase chemistry on the micromechanical processes affecting the overall behavior of the composites discussed.

5. Discussion

5.1. Residual stresses acting on a phase boundary

A theoretical estimation of the (average) residual stresses, arising from cooling down to room temperature after HIPing, will be first attempted and compared with the experimental results. A suitable start is to locate the total average stress, $\langle \sigma^i \rangle$, acting along the

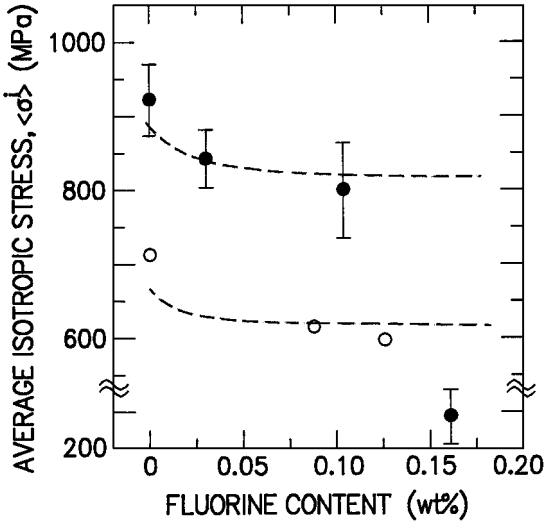

Figure 6 Experimental values of residual stress (from Raman spectroscopy measurements) as a function of the F content. The symbols are the same as those of Fig. 3. The broken lines represent the theoretical predictions of residual stress calculated as explained in Section 5.1 of the text.

direction normal to a phase boundary as

$$\langle\sigma^i\rangle = \langle\sigma^i\rangle_{TS} + \langle\sigma^i\rangle_{BS} \tag{1}$$

where the stress components located by the subscripts TS and BS are those arising from the mismatch in thermal expansion coefficients of the neighboring phases and the elastic back-stress associated with the cooling process under high pressure, respectively.

Under the assumption that the spatial and angular distributions of the dispersoid crystals in the matrix are random, the average isotropic part of the residual stress in the matrix, $\langle\sigma^i\rangle_m$, and the dispersoid phases, $\langle\sigma^i\rangle_d$, can be expressed and related by a force balance condition according to the following expressions [30]:

$$\langle\sigma^i\rangle_m = [3K_mK_d/V_{fm}(K_m - K_d)]\{V_{fd} - [K_d(K_m - K^*)/ K^*(K_m - K_d)]\}(\alpha_m - \alpha_d)\Delta T \tag{2}$$

$$V_{fm}\langle\sigma^i\rangle_m + V_{fd}\langle\sigma^i\rangle_d = 0 \tag{3}$$

where V_f, K and α are the volume fraction, the bulk modulus, and the average thermal expansion coefficient, respectively; the subscripts m and d locate the parameters which refer to matrix and dispersoid, respectively. The elastic stress-free temperature (upon cooling), ΔT, is assumed to equal the relaxation temperature of the glassy-SiO_2 phase-boundary (i.e., $\Delta T = T_R$) and, hence, is a function of the F content (cf. Fig. 2). At first approximation, the precise temperature dependence of the thermal expansion coefficients was neglected and an average thermal mismatch value, $\langle\Delta\alpha\rangle = (\alpha_m - \alpha_d)_{av}$, considered. The $\langle\Delta\alpha\rangle$ value was assumed as 0.85 and $0.50 \times 10^{-6}\,^{\circ}C^{-1}$ for SiC and WC dispersoids, respectively. The effective bulk modulus, K^*, is a function of the elastic constants of the constituent phases, their respective volume fractions, and topological arrangement. Provided that the microstructures of the present composite materials are statistically isotropic and, moreover, considering the relatively low volume fraction of dispersoid added in the present study, the effective bulk modulus can be expressed as the upper Hashin limit, K^+, given by the equation [30]:

$$K^* = K^+ = V_{fm}K_m + V_{fd}K_d - \left[V_{fm}V_{fd}(K_m - K_d)^2/ (V_{fm}K_d + V_{fd}K_m + 4G_m/3)\right] \tag{4}$$

where G_m is the shear modulus of the matrix. The average residual stress acting on the phase boundary, as a consequence of thermal expansion mismatch, was assumed as $\langle\sigma^i\rangle_{TS} = \langle\sigma^i\rangle_d$, the latter term being computed according to Equations 1–4.

An elastic back-stress component, $\langle\sigma^i\rangle_{BS}$, may arise from the cooling process under high isostatic pressure. The dispersoids, embedded into the matrix, are hydrostatically compressed for an amount of strain equal to p/K_d, where p is the externally applied isostatic pressure while sintering. Upon cooling, internal equilibrium is achieved between the stress components deriving from thermal expansion mismatch and those arising from the externally applied pressure. Hence, the dispersoids, in elastically compressed status, are cooled down below the relaxation temperature, $T_R = \Delta T$, of the grain-boundary phase. It can be conceived that the grain-boundary SiO_2-phase acts as a "glue" between neighboring crystals. When the sintered composite body is cooled down to room temperature, this phase transforms from the liquid to the solid status, its viscosity being lowered according to a known exponential temperature dependence (i.e., Fig. 2B). Once the grain-boundary phase is cooled down to a temperature $T < T_R$, local grain-boundary sliding cannot be anymore allowed and local stress relaxation is thus inhibited. This means that the SiO_2 grain-boundary phase will "glue" the dispersoids into the matrix in their compressively deformed status. An explanatory schematic of this mechanism leading to elastic back-stress upon HIPing process, is shown in Fig. 7. Thus, when the external pressure is released, the elastic back-stress will result as:

$$\langle\sigma^i\rangle_{BS} = (K_m/K_d)p \tag{5}$$

This stress component will act on the phase boundaries in compressive fashion. The expression of elastic back-stress, as given by Equation 5, neglects any anisotropy of the elastic constants of the dispersoids as well as their plastic deformation below the relaxation temperature of the grain-boundary phase. This latter approximation was thought to be plausible for highly refractory phases such as SiC and WC. Note that, under the present assumption of negligible change in compressibility of solid SiO_2 upon F addition, $\langle\sigma^i\rangle_{BS}$ is independent of the F content. Broken lines in Fig. 6 show the total residual stress, $\langle\sigma^i\rangle$, which acts on a phase boundary as theoretically calculated from Equations 1–5. The dependence on the F content arises from the change in (elastic) stress-free temperature (on cooling), ΔT, namely the temperature at which the glassy-SiO_2 phase-boundary relaxes (cf. Fig. 2B). A reasonable agreement seems to be achieved with the experimentally determined

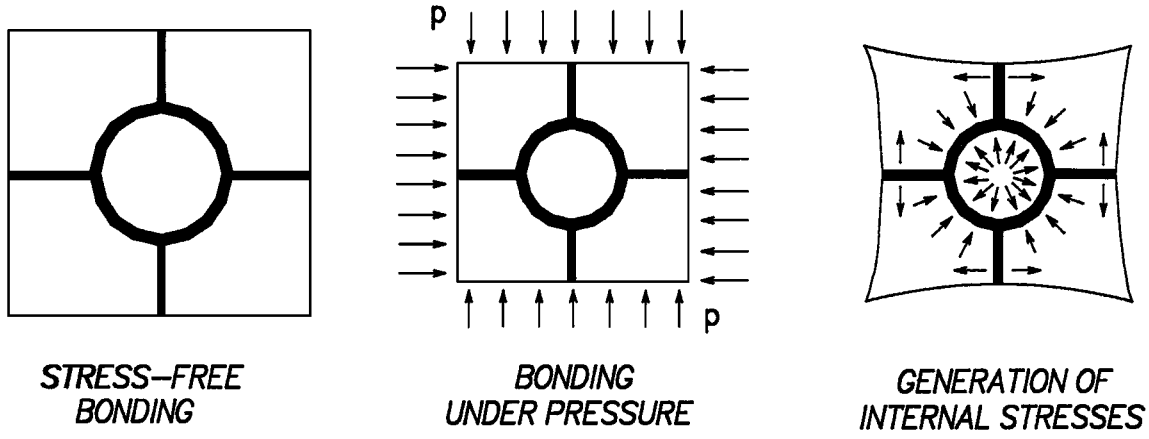

Figure 7 Explanatory draft of the residual (elastic) back-stress caused by cooling under high pressure, p, a composite whose constituent phases own a mismatch in elastic properties. The black film circumventing the inclusion in the draft represents the boundary phase which, for simplicity's sake, is assumed to be incompressible in the present analysis.

stress data for low amounts of F dopant. More importantly, the theoretical curves seem to correctly predict the strongly non-linear dependence of the residual microstresses on the F content. On the other hand, residual (tensile) stress values much higher than those actually found by spectroscopic experiments are predicted for large F amounts. According to TEM observation (Fig. 5), such a discrepancy between experimental and theoretical values can be attributed to microcrack formation, which locally releases the microstresses acting on the phase-boundaries. The possibility that a threshold value exists for the fraction of F in the glassy-SiO_2, above which microcracks can be formed, is theoretically explored hereafter.

5.2. Critical F content for phase-boundary microcrack formation

To assess the critical content of F, x_F^*, for which spontaneous microcracking can occur in the composite body, an analysis based on both fracture mechanics principles and concepts of glass-network theory is followed. First, the fracture mechanics problem of an isolated slit-like crack placed (at random orientation) within the glassy-SiO_2 film between matrix and platelet is addressed. Then, the actual structure of the SiO_2-glass network, as modified by the F dopant, is taken into consideration. According to the glass-network theory [9, 31], a law relating the size of an *equivalent* crack (or flaw) in the SiO_2 structure to the amount of F incorporated into the glass network is given. These analytical procedures will allow us to discuss the micromechanical implications for the existence of a critical F-content, x_F^*, in the composites.

The critical stress intensity factor for microcrack formation in a regular array of hexagonal grains is generally assessed by considering the stress amplification at triple-grain junctions [29, 32]. However, the present microstructural arrangement appears to be quite different from the aforesaid regular array of grains, since the dispersoid platelet-phase typically displays an average dimension more than one order of magnitude larger as compared with the matrix grains (cf. Fig. 1A). Furthermore, no significant residual microstresses are thought to operate between adjacent matrix grains, since the correspondent mismatch in thermal expansion is zero. Instead, flat edges are envisaged, which are loaded in tension as a consequence of the lower thermal expansion coefficient of the matrix material compared to that of the platelets. Hence, the surrounding matrix is assumed to be a continuous medium and the stress accumulation at the triple-grains junctions is neglected. Assuming plane strain conditions, a SiO_2 phase-boundary of thickness, $2h$, and elastic constants E_g and ν_g, is considered to be perfectly bonded between two half-planes loaded with a normal traction, $\langle\sigma\rangle$. A schematic of the fracture mechanics problem is depicted in Fig. 8. A

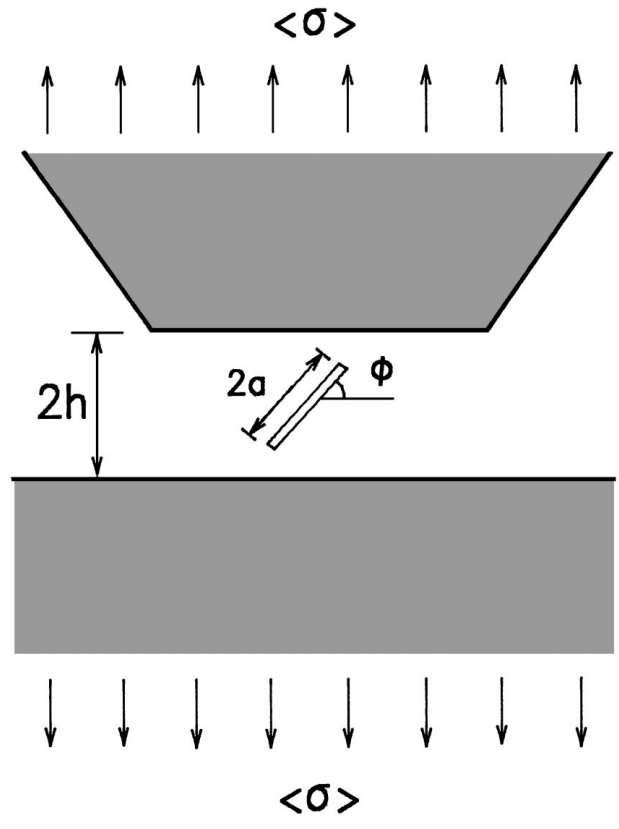

Figure 8 Explanatory draft of the fracture mechanics problem considering an arbitrarily oriented crack of size, $2a$, embedded into the boundary of two adjacent grains subjected to traction, $\langle\sigma\rangle$.

TABLE I Elastic constants of the investigated ceramic phases

Materials	Young's modulus	Shear modulus	Poisson's ratio	Bulk modulus
SiO_2	72 GPa	—	0.21	—
WC	440	—	0.26	306
Si_3N_4	310	120	0.23	193
SiC	430	—	0.26	333

small crack of length, $2a$, is placed at a random angle, ϕ, within the phase-boundary. For simplication, both Young's moduli and Poisson's ratios were taken to be the same for the two half-planes and equal to the arithmetic averages, E_{av} and ν_{av}, respectively, of those of the matrix and the platelet phases (Table I). The bulk elastic properties of the boundary phase were taken as those of pure SiO_2 glass [33] and were considered to be not affected by the F content. Since the lack of symmetry of the arbitrarily oriented crack problem, the analytical solution for any arbitrary orientation angle, ϕ, of the crack respect to the boundaries, is very complex [34]. In this paper, the fracture mechanics problem is bound between two extreme cases: (I) a crack parallel to the bond lines ($\phi = 0^\circ$) and, (II) a crack normal to them ($\phi = 90^\circ$). It has been shown that the results for intergranular cracks at intermediate angles can be considered to lie between the results for these two limiting cases [35]. We will discuss afterwards that such an approximation does not alter the final results of the theoretical assessment.

Following Hilton and Sih [34, 35], the stress intensity factor, K_I, for the crack configuration depicted in Fig. 8 can be set in the usual Griffith's fashion as:

$$K_I = Y(\phi, a/h, E_{av}, E_g, \nu_{av}, \nu_g)\langle\sigma\rangle(2a)^{1/2} \quad (6)$$

where the coefficient Y is function of the crack inclination angle ϕ, the ratio of the crack length to the phase-boundary thickness, a/h, and the elastic constants of both the intergranular SiO_2 phase and the surrounding crystals. The function Y is then determined for the particular cases $\phi = 0^\circ$ and 90°. For brevity's sake, only the equations pertinent to the case of a crack parallel to the phase boundary (i.e., $\phi = 0^\circ$) are explicitly shown hereafter, the coefficient Y for the case $\phi = 90^\circ$ being derived with a similar procedure [34]. The coefficient Y is, by definition:

$$Y = \lim_{t\to 1}\left[t^{1/2} - \int_0^1 k(t,s)\Phi(s)\,ds\right] \quad (7)$$

where

$$k(t,s) = (ts)^{1/2}\int_0^\infty \xi[f(\xi) - 1]J_0(\xi t)J_0(\xi s)\,d\xi \quad (8)$$

$$\Phi(\tau) = (2/\pi)\int_0^x [p/(\tau^2 - x^2)]\,dx - \int_0^a \rho\Phi(\rho) \times \int_0^\infty \xi[f(\xi) - 1]J_0(\xi t)J_0(\xi s)\,d\xi\,d\rho \quad (9)$$

in which t, s, and ρ are auxiliary variables of the abscissa x, whose origin is placed at the center of the intergranular crack, $\xi = as$, and $\tau = at$. $k(t,s)$ is the symmetric kernel, while J_0 is the Bessel function of the first kind of order zero. $\Phi(\xi)$ is a function of the elastic constants (of both SiO_2 film and adjacent grains) and of the SiO_2-film thickness, given as [35]:

$$\Phi(\xi) = \{a + [\beta(\xi h)^2 + \gamma]\exp(-2\xi h) + \delta\exp(-4\xi h)\}/\{a - \beta(\xi h)\exp(-2\xi h) - \delta\exp(-4\xi h)\} \quad (10)$$

with

$$\alpha = (1/2E_g^2)[3 - 4\nu_g + (3 - 4\nu_m)(E_g/E_m)^2 + 2(5 - 6\nu_g - 6\nu_m + 8\nu_g\nu_m)(E_g/E_m)] \quad (11)$$

$$\beta = (2/E_g^2)[1 - (3 - 4\nu_m)(E_g/E_m)^2 + 2(1 - 2\nu_m)(E_g/E_m)] \quad (12)$$

$$\gamma = (1/E_g^2)\left[(5 - 12\nu_g + 8\nu_g^2) - (3 - 4\nu_m)(E_g/E_m)^2 - 2(1 - 2\nu_g - 2\nu_m + 4\nu_g\nu_m)(E_g/E_m)\right] \quad (13)$$

$$\delta = (1/2E_g^2)[3 - 4\nu_g + (3 - 4\nu_m)(E_g/E_m)^2 - 2(3 - 2\nu_g - 2\nu_m)(E_g/E_m)] \quad (14)$$

The above system of integral equations has been numerically solved. Fig. 9 shows a plot of the coefficient Y as a function of the ratio a/h, which was calculated from Equations 6–14 (and the correspondent equations for $\phi = 90^\circ$ [34]) by introducing the appropriate elastic constants and phase-boundary thickness for the present materials (cf. Table I). Between the two curves, which refer to the inclination angles $\phi = 0^\circ$ and $\phi = 90^\circ$ and bind the Y values for any possible inclination angle, the most severe situation is proved to be that of a crack placed parallel to the phase-boundary (i.e., $\phi = 0^\circ$). The broken lines $Y = 1$ and $Y = E_g(1 - \nu_m)/E_m(1 - \nu_g)$, also shown in Fig. 9 for comparison, represent the limiting cases of h/a approaching infinity and zero values, respectively, for a crack parallel to the interface [35]. From a physical point of view, the case of h/a approaching infinity corresponds to an homogeneous

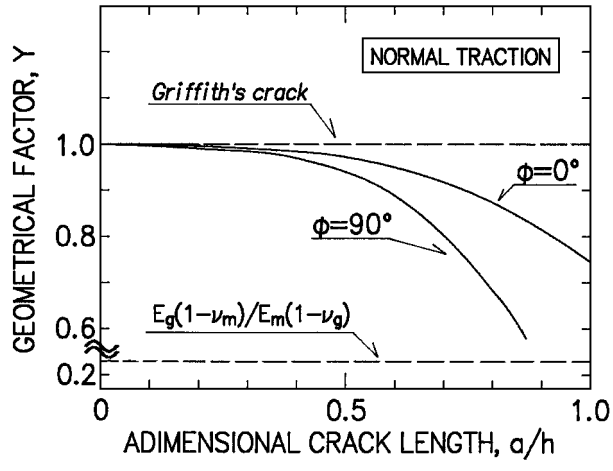

Figure 9 Geometrical factor, Y, for the crack configuration shown in Fig. 8. Values for two limiting conditions, $\phi = 0^\circ$ and $\phi = 90^\circ$, are shown. All the Y values are bound between the cases of a Griffith's crack ($h/a \to \infty$), and imperfect bonding of a very thin boundary ($h/a \to 0$).

glass sheet which contains a crack of size, $2a$ (i.e., the classic Griffith's problem). On the other hand, the case $h/a \to 0$ represents two adjacent grains bonded imperfectly along a straight boundary of very small but finite thickness. The calculations shown in Fig. 9 provide the basis to assess whether or not spontaneous microcracking occurs in the composites upon F addition. Since the case $\phi = 0^\circ$ is proved to be the most severe (i.e., leading to higher local stress intensity factor, K_I), only this interfacial crack configuration will be discussed hereafter.

Let us now envisage the phase-boundaries as being filled and strongly bonded with a network-structured medium, namely the pure SiO_2 glass, whose atomistic structure is modified by the presence of F (cf. Fig. 1). The presence of each two F anions will involve one Si-O broken bond in the network. It can be thought that an *equivalent* unitary crack of size $a_0 \approx 0.53$ nm (i.e., equal to the average size of a single SiO_2-glass cluster) is associated to each Si-O broken bond. Note that the size of a unitary crack a_0 is not negligible as compared to the phase-boundary width (i.e., $h/a_0 \approx 8$). With increasing the F amount, x_F, the non-bonded sites within the SiO_2 network will increase until they typically reach a percolation threshold, x_F^*. In other words, adding a fraction of F-dopant to the composite can be thought to correspond to a "mechanistic" process of randomly cutting a certain fraction of bonds in the network which "glues" two neighboring crystals and, thus, to create a number of interfacial cracks. For $x_F = x_F^*$, the degree of coherence of the network [33] is annihilated and the phase boundary results basically unbonded on the atomic scale. Invoking basic principles of glass-network theory [9, 33], it can be shown that the F-amount for which each glass cluster owns one non-bonded site and, hence, the glass network in the intergranular film results to be fully percolated, should be at around $x_F^* \approx 15$ at % F-content in the glassy-SiO_2 film (i.e., ≈0.30 wt % F in the composite). In other words, x_F^* represents the threshold value of F content for which an infinitely long (percolated) chain of broken bonds can exist in the glass network. The (statistical) average size of an *equivalent* inter-granular crack, $2a_e$, can then be set as [36]:

$$2a_e = A/[(x_F^* - x_F)/2]^t \qquad (15)$$

where the F amounts x_F^* and x_F are in at % in SiO_2, the multiplying factor $1/2$ arising from the need of two F ions per each Si-O broken bond. The exponent t, independent of the structural details of the network, is found to experience the value 1.35 for a two-dimensional glass network† [37], while a value 0.160 can be found for the constant A with imposing the condition $2a_e = a_0$ for $x_F = 0$. The *equivalent* crack size, $2a_e$, as a function of the F concentration, x_F, in SiO_2 is plotted in

† Note that the exponent $t = 1.35$ in the percolation law [37] has been by purpose selected as that of a bidimensional glass-network structure. This choice would imply that, in the planar fracture mechanics problem considered in Fig. 8, the plane of applied tension has to be selected for each boundary as coincident to the plane within which the intergranular crack lies, any non-planar configuration of the crack being neglected.

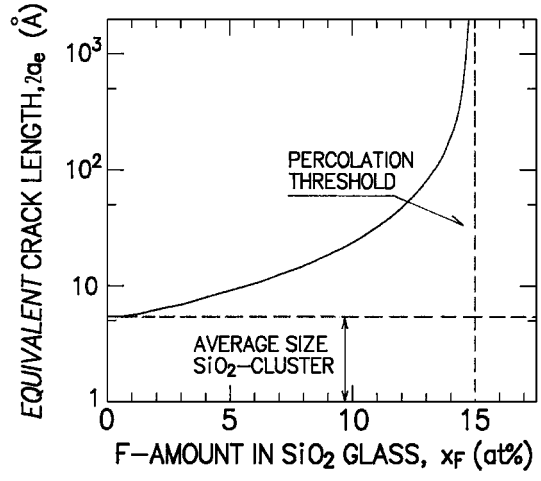

Figure 10 *Equivalent* length, $2a_e$, of a phase-boundary crack as a function of the F-content, x_F. The function is established according to the probability approach described in Section 5.2.

Fig. 10. Combining the fracture mechanics results from Equations 6–14 (i.e., the plot for $\phi = 0^\circ$ in Fig. 9) with the statistical crack length of Equation 15 (i.e., Fig. 10), and enforcing the theoretical dependence of the residual stress, $\langle \sigma^i \rangle$, upon x_F (cf. broken lines in Fig. 6), an equation relating the stress intensity factor, associated with an isolated intergranular crack, $K_I^{(s)} = Y \langle \sigma \rangle (2a_e)^{1/2}$, and the F amount, x_F, can be found. This relation is shown in Fig. 11, for the Si_3N_4/SiC composite. Two straight lines are also drawn to envisage the interval within which the bulk value of toughness, K_{Ic}, of the SiO_2 glass was experimentally found upon F addition. The interceptions of the K_{Ic} lines with the $K_I^{(s)}$ curve locate a (narrow) abscissa interval of critical F-concentrations (i.e., of critical *equivalent* microcrack size) above which a percolated chain of broken Si-O bonds can propagate unstably upon cooling down from HIPing temperature. This propagation will generate a microcrack of size comparable with that of the platelet dispersoid. Obviously, the case of an isolated crack of length, $2a_e$, at the interface may have little statistical relevance when a homogeneous distribution of F-dopant is

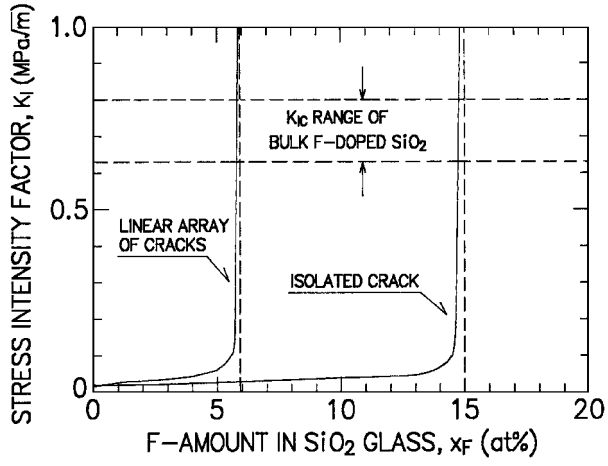

Figure 11 Theoretically determined stress intensity factor, K_I, associated to the coalescence process of non-bridged SiO_2 clusters, as a function of the F-amount in SiO_2 glass. Two limiting cases corresponding to the configuration of an isolated and an infinite array of cracks are considered. The experimental K_{Ic} range found for F-doped glass is also shown for comparison.

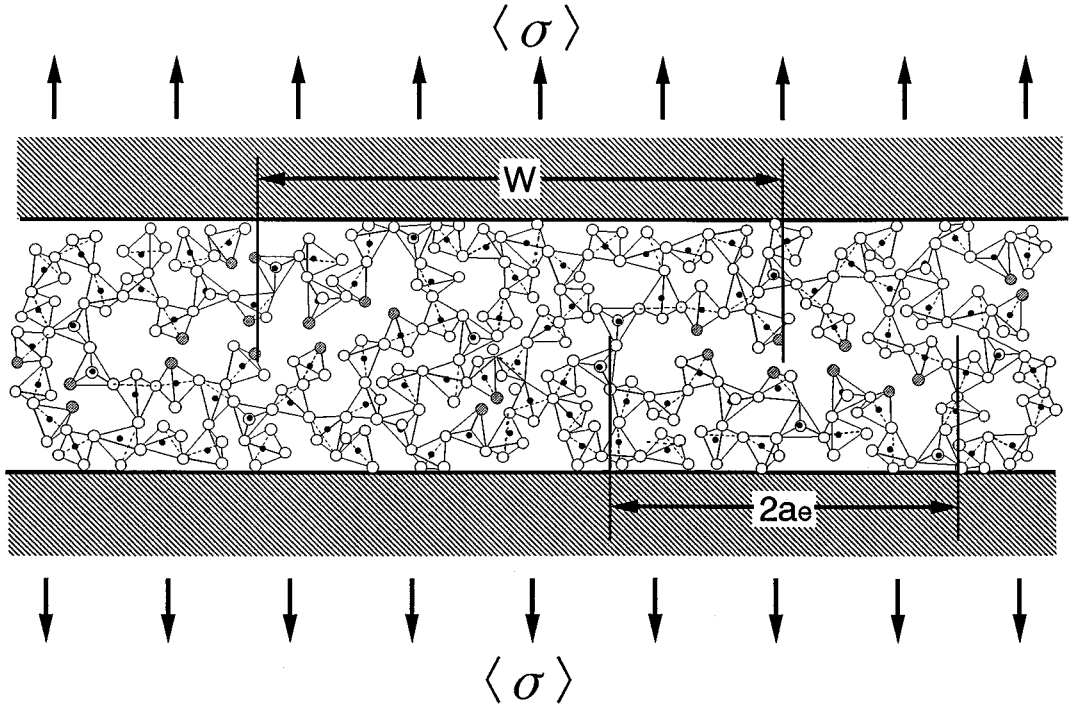

Figure 12 Linear array of coalesced non-bridged SiO_2 clusters (i.e., equivalent cracks) in the SiO_2 network at the phase boundary. The geometrical parameters used in the fracture mechanics calculation are also envisaged. F atoms are depicted as shaded circles, while close and open circles locate Si and O atoms, respectively.

present along the interfacial glassy film. Hence, the $K_I^{(s)}$ curve for an isolated crack in Fig. 11 can only represent a lower boundary solution of the actual micro-cracking problem. A more realistic picture of the glass interface doped with F will envisage the glassy film as containing two or more aligned cracks of length, $2a_e$. A schematic of the cracked SiO_2-network is depicted in Fig. 12. In order to assess an upper boundary for the K_I value of the cracked interface, an infinite array of planar cracks is considered, in which the ratio $\kappa = 2a_e/W$ represents the fraction of cracked interface (cf. Fig. 12) and is dictated by the statistically "worst" crack configuration. Such a configuration consists of all cracks of length $2a_e$, perfectly aligned along the interface (i.e., $\phi = 0^\circ$). In addition, the ratio κ is set equal to the fraction of "open" SiO_2 clusters per unit interface length[‡], namely:

$$\kappa = n_b/n_t = (x_F/2)\varepsilon * 2ha_0 \qquad (16)$$

where n_b is the number of non-bridged SiO_2 clusters per unit length and $n_t = 1/a_0$ is the total number of SiO_2 clusters per unit length; the phase-boundary thickness is taken as $2h \approx 4$ nm and $\varepsilon = 16.12$ nm^{-2} is the number of Si-O bonds per unit area of SiO_2 network [38]. The stress intensity factor associated with the crack array, $K_I^{(a)}$, is then given as [39]:

$$K_I^{(a)} = 0.826\, K_I^{(s)}[\pi/(1-\kappa)]^{1/2} \qquad (17)$$

From Equations 16 and 17 and the $K_I^{(s)}$ curve of Fig. 11, the upper-limit stress intensity factor, $K_I^{(a)}$, for the phase-boundary crack array can be calculated as a function of the F content. The results of this calculation are displayed in Fig. 11. The crack-array configuration leads to a a critical F content in $SiO_2 \approx 5.9\%$. It is conceivable that the actual stress intensity factor for all the possible phase-boundary crack configurations displays a value $K_I^{(s)} < K_I < K_I^{(a)}$. The critical F content, $x_F^* \approx 8.1$ at %, experimentally found for the present composites, reasonably lies between the theoretically predicted values. The theoretical analysis appears also able to consistently explain the presence of a spontaneous process of phase-boundary microcracking as experimentally found for large additions of F-dopant, in spite of the fact that the bulk toughness of the intergranular glassy phase is not markedly altered by the incorporation of F. The theoretical analysis also envisages that the decreasing of relaxation temperature of the intergranular film upon F addition, as well as the possible back-stresses associated with the cooling process under pressure, may play only a minor role on microcrack formation, as compared to the chemistry-related modification of the glass network. Both experimental and theoretical results strongly suggest that a Si-O broken-bond percolation process at the intergranular SiO_2 film is the mechanism which *amplifies* the effect of intergranular chemistry and triggers spontaneous microcrack formation in the present composites.

[‡] Note that, in the present theoretical assessment, the choice of the crack plane is not random but is dictated by the most severe configuration of the interfacial crack array. This justifies the choice of displaying a planar array of cracks whose length is a three-dimensionally averaged crack length (i.e., $2a_e$).

5.3. Macroscopic toughness of the composites

In a previous study of the present composites [12], the dependence of the macroscopic fracture energy,

WOF, on the microscopic (apparent) fracture energy of the phase boundary, γ_i, was experimentally analyzed. An order-of-magnitude estimate of the *apparent* phase-boundary energy was provided by quantitative fractography data which, for gaining statistical validity, were collected over the entire fractured surface of each composite specimen. It was found that the macroscopic fracture energy of the composite first increases while decreasing the microscopic phase-boundary energy; then, saturation occurs at around a few J/m^2 and, finally, a sudden drop-down is found within a very narrow range of γ_i values below $\approx$1 J/m^2. These experimental data are shown in Fig. 13. It can be interesting here to compare these data with those predicted by the present analysis, based on a micromechanical rather than phenomenological approach. The apparent fracture energy of the F-doped SiO_2 phase-boundary can be estimated according to the following equation:

$$\gamma_i = (K_{Ic} - \Delta K)^2(1 - \nu_g)/E_g \qquad (18)$$

where the fracture toughness of the bulk SiO_2 glass is assumed here as $K_{Ic} = 0.72$ MPa $\times$ m$^{1/2}$ (i.e., the average value found experimentally, cf. Fig. 11), independently of the F content. The factor ΔK, leading to an *apparent* decrease of bulk toughness, arises from the stress intensification due both to the presence of residual stresses and to the morphology of the glass network as modified by the F ions (cf. Fig. 12). ΔK is obviously function of x_F and should be comprised between the limiting values $K_I^{(s)}$ and $K_I^{(a)}$, the shape of the curve being the same as those of the boundary curves plotted in Fig. 11. ΔK is set equal to $K_I^{(s)}$ and, hence, calculated from Equations 15–18. Assuming $x_F^* \approx 8.1$ at %, as found experimentally, the dependence of WOF on γ_i can be obtained from the plot in Fig. 3. The results of this calculation, displayed in Fig. 13, show good agreement with the fractographic data. This may prove that the order of magnitude estimate of γ_i, which we have discussed in this study, is basically correct.

The present results support the idea that lowering the phase-boundary energy by adding, for example, a network-modifier anion to the intergranular glassy phase, may lead to an increase of the composite toughness. However, two important circumstances should be also envisaged: (I) the toughening effect, as achieved by lowering the interface energy, is a phenomenon decided according to an optimum γ_i value; (II) a decrease in γ_i of the polycrystal can be useful only in the extent that a discrete microcrack process zone can exclusively results in the neighborhood of the crack tip. As discussed in previous works on toughening mechanisms in ceramic composites [13, 40], opening of interfaces ahead of the crack tip constitutes an important precursor mechanism for toughening by crack-face bridging, which may make the material experience a rising *R*-curve behavior. The occurrence of rising *R*-curve behavior is indeed the main micromechanical reason which leads to the increase in macroscopic fracture energy in the present composite system [6]. However, when a threshold fraction of network-modifier dopant is exceeded, spontaneous microcracking is allowed to occur upon cooling all over the polycrystal and the fracture energy may drop down together with the material stiffness, the composite body being ultimately unbonded on the microstructural level.

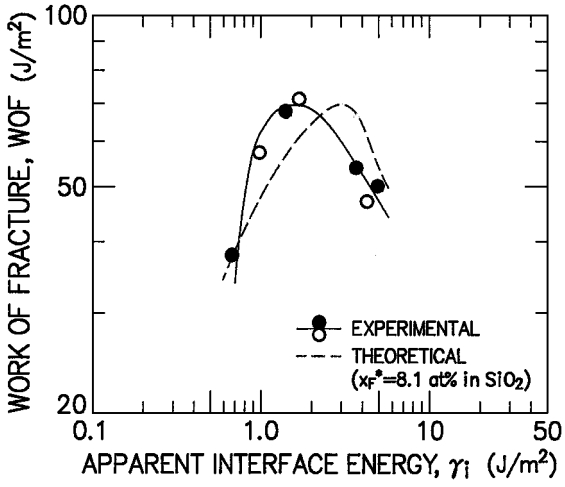

Figure 13 Macroscopic fracture energy, WOF, of the composite as a function of the *apparent* interface energy, γ_i, as both experimentally and theoretically determined according to fractographic data and the percolation model described in Section 5.2, respectively.

6. Conclusion

The influence of a systematic modification of the interface chemistry on the mechanical properties of Si_3N_4-based composites was investigated. It is shown that the addition of F anions, which modify the SiO_2-glass network, can lead to spontaneous microcrack formation which, in turn, may markedly alter both the stiffness and the macroscopic fracture energy of the material. In this study, emphasis was placed on assessing the major mechanism which leads to microcrack formation and in exploring as to whether a threshold value exists for the F amount in the SiO_2 phase-boundary film which causes spontaneous microcrack formation upon cooling. Both experimental and theoretical assessments of the phenomenon suggest that, in the present composites, the most critical circumstance which leads to the formation of spontaneous microcracking is a chemistry-related intensification of the residual (tensile) microstress acting on the phase boundaries. The tensile stress arises from the mismatch in thermal expansion coefficients of the constituent phases. Although the magnitude of the residual stress may be not sufficient to cause fracture in undoped phase boundaries, local stress intensification can occur as a consequence of an atomic-scale percolation process in the F-doped SiO_2 network. This local stress intensification is found to trigger spontaneous phase-boundary fracture and to affect the macroscopic mechanical behavior of the composite.

Acknowledgements

Part of this work has been supported by the Mitsubishi Foundation. The authors gratefully thank Professor M. Rühle and Professor M. Sakai for valuable discussions and for encouraging the present work. Dr. G. Katagiri and Mr. K. Tanabe at Toray Research Laboratories are sincerely acknowledged for the support

of Raman spectroscopy and the ISE analyses, respectively. The help of Mr. Y. Hatano and Mr. T. Hashimoto in the experimental procedures is also gratefully acknowledged.

References

1. F. F. LANGE, *J. Amer. Ceram. Soc.* **56** (1973) 445.
2. M. MITOMO and S. UENOSONO, *ibid.* **75** (1992) 105.
3. A. PYZIK and D. R. BEAMAN, *ibid.* **76** (1993) 2737.
4. I. M. PETERSON and T.-Y. TIEN, *ibid.* **78** (1995) 2345.
5. I. TANAKA, G. PEZZOTTI, K. MATSUSHITA, Y. MIYAMOTO and T. OKAMOTO, *ibid.* **74** (1991) 752.
6. G. PEZZOTTI, *ibid.* **76** (1993) 1313.
7. H.-J. KLEEBE, M. K. CINIBULK, I. TANAKA, J. BRULEY, J. S. VETRANO and M. RÜHLE, in "Tailoring of Mechanical Properties of Si_3N_4 Ceramics", edited by M. J. Hoffmann and G. Petzow (Kluwer Academic Publications, The Netherlands, 1994) pp. 259–74.
8. G. PEZZOTTI, K. OTA and H.-J. KLEEBE, *J. Amer. Ceram. Soc.*, submitted.
9. S. H. RISBUD, *Phys. Chem. Glass.* **22** (1981) 168.
10. G. PEZZOTTI, K. OTA, H.-J. KLEEBE, Y. OKAMOTO and T. NISHIDA, *Acta Metall. Mater.* **43** (1995) 4357.
11. H.-J. KLEEBE, G. PEZZOTTI and T. NISHIDA, *J. Mater. Sci. Lett.*, in press.
12. G. PEZZOTTI, H.-J. KLEEBE, K. OTA, T. NISHIDA and M. SAKAI, *J. Ceram. Soc. Jpn.* **104** (1996) 17.
13. G. PEZZOTTI, *Acta Metall. Mater.* **41** (1993) 1825.
14. G. PEZZOTTI, I. TANAKA and T. NISHIDA, *Phil. Mag. Lett.* **67** (1993) 95.
15. I. TANAKA, G. PEZZOTTI, Y. MIYAMOTO and T. OKAMOTO, *J. Mater. Sci.* **26** (1991) 208.
16. V. SERGO, G. PEZZOTTI, N. MURAKI, G. KATAGIRI and T. NISHIDA, *J. Amer. Ceram. Soc.* **79** (1996) 781.
17. G. PEZZOTTI, V. SERGO, N. MURAKI, K. OTA, M. SAKAI and T. NISHIDA, *J. Ceram. Soc. Jpn.* **104** (1996) 497.
18. K. OTA and G. PEZZOTTI, *Scripta Metall. Mater.* **33** (1995) 1177.
19. *Idem., Phil. Mag.* **A73** (1996) 223.
20. *Idem., Scripta Metall. Mater.* **34** (1996) 1467.
21. G. PEZZOTTI, K. NIIHARA and T. NISHIDA, *J. Testing Eval.* **21** (1993) 358.
22. Japan Industrial Standard, Testing Method for Fracture Toughness of High-Performance Ceramics JIS *R*1607 (Japanese Standards Association, Tokyo, 1990).
23. T.-S. KÊ, *Phys. Rev.* **71A** (1947) 533.
24. A. S. NOWICK and B. S. BERRY, "Anelastic Relaxation in Crystalline Solids" (Academic Press, New York, 1972) p. 52.
25. H.-J. KLEEBE, M. K. CINIBULK, R. M. CANNON and M. RÜHLE, *J. Amer. Ceram. Soc.* **76** (1993) 1969.
26. E. FEHER and M. D. STURGE, *Phys. Rev.* **172** (1968) 244.
27. J. F. DI GREGORIO, T. E. FURTAK and J. J. PETROVIC, *J. Appl. Phys.* **71** (1992) 3524.
28. L. GRABNER, *ibid.* **49** (1978) 580.
29. Y. FU and A. G. EVANS, *Acta Metall.* **33** (1985) 1515.
30. W. KREHER and W. POMPE, "Internal Stresses in Heterogeneous Solids" (Akademie-Verlag, Berlin, 1989).
31. J. M. STEVELS, *Handbk. Phys.* **XIII** (1962) 510.
32. A. G. EVANS, *Acta Metall.* **26** (1978) 1845.
33. S. SAKKA, T. SAKAINO, K. TAKAHASHI and N. SOGA, "Glass Handbook" (Asakura Shoten, Tokyo, 1980) p. 657.
34. P. D. HILTON and G. C. SIH, *Int. J. Solids Structures* **913** (1971).
35. Idem. in Proceedings: Fifth Southeastern Conference on Theoretical and Applied Mechanics (Pergamon Press Publisher, New York, 1971) pp.123–149.
36. R. ZALLEN, "The Physics of Amorphous Solids" (John Wiley & Sons, Inc., New York, 1983) p. 157.
37. H. TAKAYASU, "Fractal Science" (Asakura Shoten, Tokyo, 1987) p. 175.
38. R. B. SOSMAN, "The Phases of Silica" (Rutgers University Press, New Brunswick, 1965) p. 290.
39. J. P. BENTHEM and W. T. KOITER, in "Methods of Analysis of Crack Problems," edited by G. C. Sih (Nordhoff, Leyden, 1972) p. 131.
40. G. PEZZOTTI, Y. OKAMOTO, T. NISHIDA and M. SAKAI, *Acta Metall. Mater.* **44** (1996) 899.

Received 19 April 1996
and accepted 20 October 1998